Mon. Not. R. astr. Soc. (1987) **225,** 653–675

Dissection of an *N*-body bar

Linda S. Sparke *Kapteyn Laboratory, Postbus 800, 9700 AV Groningen, The Netherlands*

J. A. Sellwood *Department of Astronomy, The University, Manchester M13 9PL*

Accepted 1986 October 29. Received 1986 October 29; in original form 1986 September 22

Summary. We present a detailed study of a two-dimensional *N*-body bar formed through a global disc instability. The rapidly tumbling figure is made up almost exclusively of orbits trapped or semi-trapped about the main family of prograde periodic orbits, which is aligned with the long axis of the bar. The bar also appears to be stable and is very robust. Iso-density contours of the mass distribution are nearly rectangular, and differ markedly from the elliptical shape commonly assumed for bars.

1 Introduction

A great deal of effort in recent years has resulted in quite detailed knowledge of the types of orbits to be expected in rapidly tumbling barred potentials. Many authors (e.g. Contopoulos 1980; Petrou 1984; Teuben & Sanders 1985) have noted that the time-averaged space density of some orbit families is generally elongated in the direction of the bar major axis, while other families would make an entirely different, less favourable, contribution. They concluded that a self-consistent bar might be made up largely of stars following these favourable orbit families.

Schwarzschild (1979) successfully applied linear programming techniques to construct a fully self-consistent model of a tri-axial non-rotating elliptical galaxy model. He also obtained a number of solutions for slowly rotating ellipsoids, but despite a very systematic search he did not succeed in a similar project for a rapidly tumbling, highly tri-axial bar model (private communication). Schwarzschild's approach is to take an assumed mass distribution, guess a figure rotation speed and compute a large number of orbits in the potential. He then asks whether some non-negative combination of the time-averaged orbits would add up to the density distribution of the assumed mass model.

N-body experiments lead one to believe that bars should be rather easy to construct. Rapidly tumbling bars have frequently been obtained in both 2-D (e.g. Miller & Prendergast 1968; Hohl 1971; Sellwood 1981) and 3-D (e.g. Miller & Smith 1979; Hohl & Zang 1979) simulations. Many of these are fully self-consistent, although the bars are not isolated – sometimes they are embedded within a disc or a bulge or they may be surrounded by a halo of particles. These bars

appear to be long-lived, but several authors (e.g. Combes & Sanders 1981; Carnevali 1983) have commented that pattern speed or amplitude may decay in a secular fashion.

The failure of Schwarzschild's approach may indicate merely that there is no solution for his original choices of figure shape and rotation rate, but the problem could be more fundamental; there may be no fully self-consistent, stable, rapidly rotating configurations for isolated stellar systems. Perhaps all rapidly tumbling bars slowly evolve.

Pfenniger (1984b), on the other hand, describes a 2-D model for a rapidly tumbling bar, using a least-squares approach to the self-consistency requirement. He found solutions with very small residuals, indicating that these models were close to self-consistent. Linear programming, however, did not yield solutions for the same problem (Pfenniger, private communication), which may indicate that the solution space is very limited.

This unsatisfactory state of affairs prompted us to study a bar formed in an N-body experiment in considerable detail. Our goals were to discover whether its orbital structure differed in any significant way from that found in the studies cited above, in which the mass model was adopted arbitrarily, and to determine more carefully whether it was in true stationary equilibrium.

In Section 2, we describe the simulation which produced our bar. We show, in Section 3, that it appears to share many of the characteristics of bars in disc galaxies. The barred potential supports most of the usual orbit families found previously, and we find in Section 4 that most particles in the bar are trapped or semi-trapped about the main long-axis family (x_1 in Contopoulos's notation). In Section 5 we demonstrate that the bar appears to be both stable and robust.

2 Construction of the bar

Rotationally supported self-gravitating discs of stars are nearly always found to be violently unstable to global bi-symmetric distortions. Simulations reveal that this instability leads to a strong and rapidly rotating bar, a result quantitatively confirmed by Inagaki, Nishida & Sellwood (1984) from a direct integration of the collisionless Boltzmann equation. [In fact, controlling this instability is one of the major problems of galaxy dynamics – see e.g. Athanassoula & Sellwood (1986) for an up-to-date review.] We have utilized this behaviour to create the bar studied here.

2.1 INITIAL CONDITIONS AND COMPUTATIONAL DETAILS

The unstable model was very similar to those described in Sellwood (1981, hereafter Paper I), but the parameters have slightly different values and the simulation was of somewhat higher quality. The initial distribution of particles was that of a Kuz'min/Toomre model disc with the radial surface density distribution:

$$\Sigma(r)=\frac{Mf}{2\pi}\,\frac{a}{(a^2+r^2)^{3/2}},$$

but truncated at $r=4a$. The central attraction of the model was supplemented by that of a rigid bulge-like component which had the density profile of a Plummer sphere:

$$\varrho(r)=\frac{3M(1-f)}{4\pi}\,\frac{b^2}{(b^2+r^2)^{5/2}}.$$

Here, M is the total mass if both distributions extended to infinity. We chose the length scales in the ratio $a:b=5:1$ and $f=0.7$ to make the disc nearly twice the mass of the bulge.

We employed 50 K particles to represent the disc with initial coordinates generated randomly from the axisymmetric disc distribution. They moved over a plane polar grid of points, introduced

to facilitate calculation of the gravitational forces, which had 70 logarithmically spaced rings and 96 equally spaced azimuthal divisions. The gravitational attraction of each particle was softened in the usual way, using a length scale of $0.1a$. The length scale a was set to 20 grid units and the time-step was $0.02(a^3/GM)^{1/2}$. In this paper we will use units such that $G=M=a=1$. Further details of the computational method are given in Paper I.

The stars were initially placed on nearly circular orbits with a small Gaussian distribution of radial velocity components chosen so as to make Q, the local stability parameter, equal to unity everywhere. The tangential velocity dispersion was set using the epicyclic formula and approximate equilibrium was established by adjusting the mean orbital speeds so as to satisfy the equation of stellar hydrodynamics.

2.2 FORMATION OF THE BAR

The evolution of the model, illustrated in Fig. 1, is very similar to those reported in Paper I. The initial prominent bi-symmetric spiral patterns lead to a bar by time 50. Continuing spiral activity gradually fades, leaving a strong, narrow, rapidly tumbling bar surrounded by a nearly axisymmetric hot outer disc of stars.

We measure the strength of non-axisymmetric features in the model by the two-dimensional Fourier transform:

$$A(m,p,t)=\frac{1}{N}\sum_{j=1}^{N}\exp\{i[m\theta_j+p\ln(r_j)]\}, \tag{1}$$

where (r_j,θ_j) are the polar coordinates of the jth particle at time t. The amplitude of $A(2,0,t)$ (the bar-like component) grows roughly exponentially, with considerable fluctuation, until time 50 (Fig. 2a) and then develops more regular oscillations about a high value. The bar amplitude is, in fact, quite steady – the periodic oscillations are due to beats with another pattern as we now show.

The rate of change of the phase of any Fourier component would be the pattern speed if only one disturbance were present. Although the bar dominates all $m=2$ features, particularly late in the run, other patterns, rotating at different rates, are present at all times. The contours in Fig. 3 show the amplitude of features in the density distribution which have well-defined angular frequencies (twice the pattern speed, since the disturbances are bi-symmetric). Fig. 3(a) and (b) relate to early and late epochs, respectively, and at least two distinct ridges are present in each.

The broad peak in Fig. 3(a) at frequencies between 1.2 and 1.5 in the inner part of the disc seems to lead to the bar, but at later times (Fig. 3b) the bar pattern speed is much lower. Fig. 3(b) also shows that the spirals in the outer disc rotate much more slowly than the bar. The period of just over 10 time units in the amplitude variations of the (2, 0) component late in the run (Fig. 2a) has the beat frequency between these two patterns. The pattern speed of the outer spiral suggests that it could be due to an edge instability (Toomre 1981).

The steadily decreasing slope in Fig. 2(b) shows that the bar does not rotate at a fixed rate even after it is well established and dominates the (2, 0) component. Between times 50 and 100 the bar pattern speed decreases from 0.5 to 0.44. A secular decrease in pattern speed was also found for the bars studied in Paper I.

The smooth curves in Fig. 3 show the radial variations of 2Ω and $2\Omega\pm\varkappa$ for the initial axisymmetric model. (Here, Ω and $\varkappa$ are the usual circular and Lindblad epicyclic frequencies for nearly circular orbits.) Thus even during the initial period, when the disturbances are comparatively weak, pattern speeds are low enough to possess inner Lindblad resonances (ILRs). Although the bars in the less centrally concentrated models of Paper I avoided them, bars

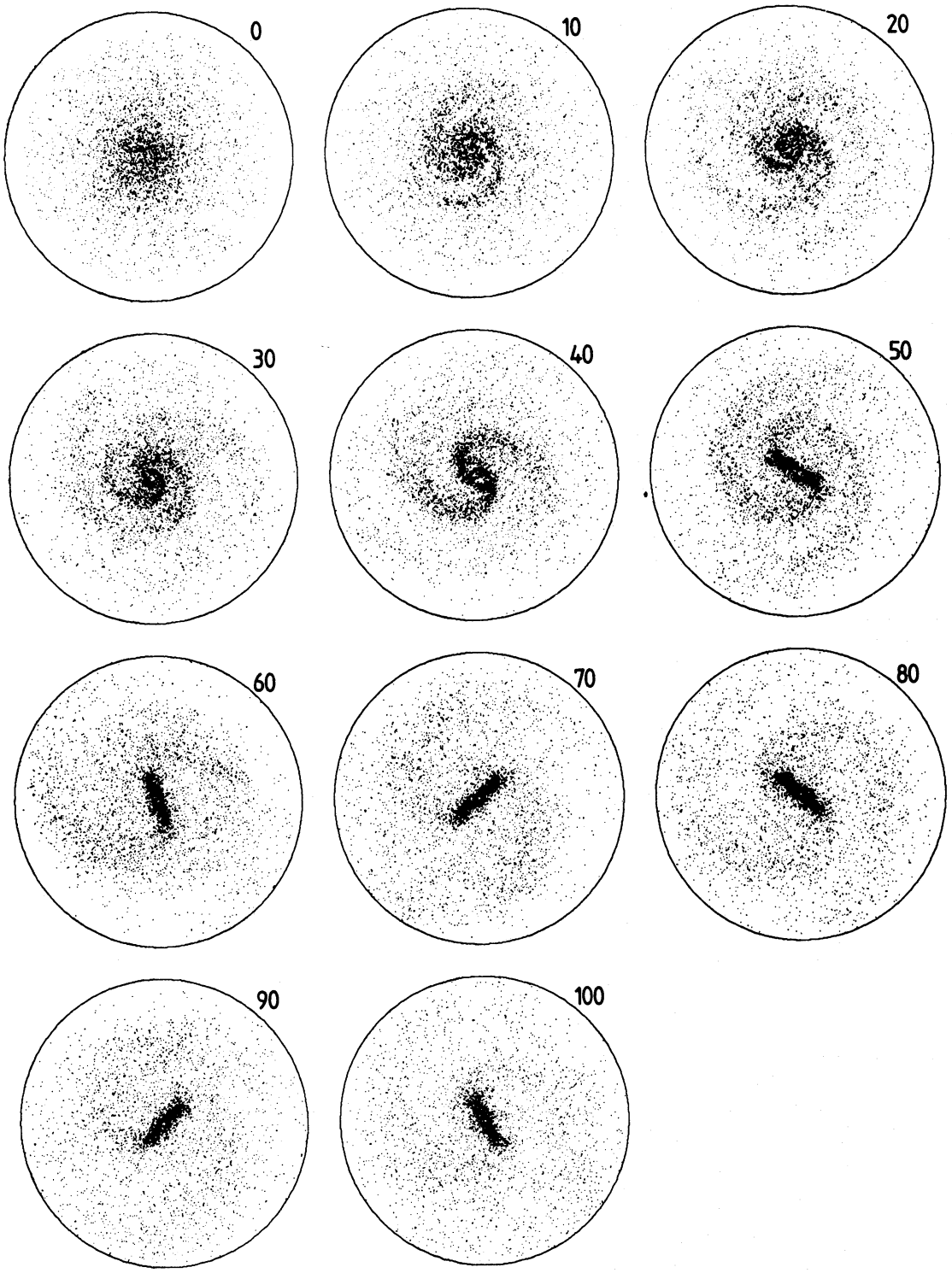

Figure 1. Development of the bar. The times are in natural units and the outer circle marks the boundary of the grid at a radius of 4.57. Only one particle in 10 is included in each frame and the bulge component is not shown.

with ILRs have formed in other cool models with dense central bulges, e.g. Zang & Hohl (1978) and Sellwood (1985). Fig. 3(b) appears to indicate that the bar possesses two ILRs, but as the potential is strongly non-axisymmetric by this time, Lindblad's condition for resonances must be generalized (see Section 4.2).

The large amplitude non-axisymmetric features of the model cause considerable rearrange-

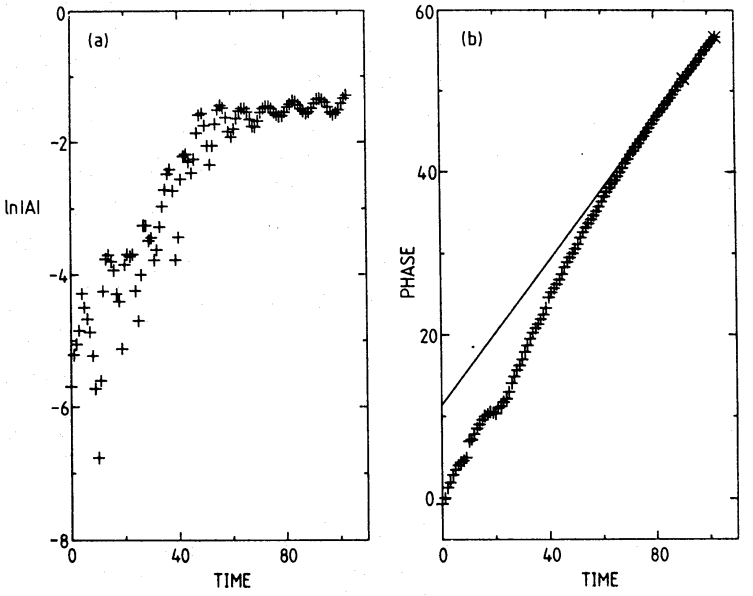

Figure 2. (a) Amplitude, and (b) phase of the bar-like (2,0) Fourier component (equation 1) of the particle distribution throughout the run. The straight line in (b) is a least-squares fit to the phases over the last part of the run. The pattern speed shows a continuing monotonic decline even after the bar is well established.

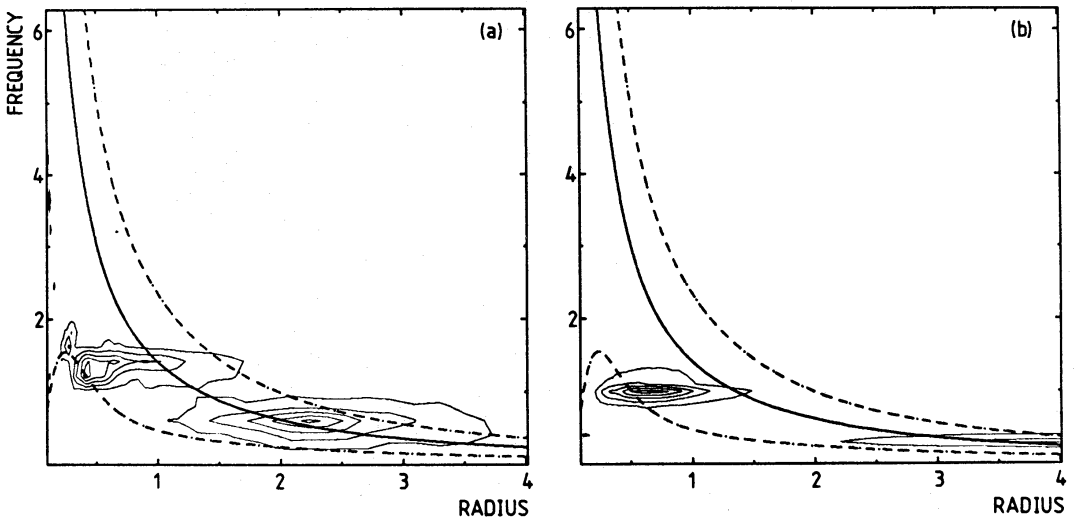

Figure 3. Contours of the square-root of power as a function of frequency and radius during (a) the early part of the run (up to time 31) and, (b) when the bar is well established (times 40 to 103). The ridges indicate the pattern speeds and radial extents of large-amplitude coherent features. The smooth curves show the radial variations of 2Ω (full drawn) and $2\Omega \pm \varkappa$ (dashed) for the initial axisymmetric model and thus are relevant only far out in the disc in (b). Both major patterns in (a) apparently rotate slowly enough to possess inner Lindblad resonances, even as the bar develops. The pattern speed of the bar, the dominant ridge in (b), is much lower than its precursive feature in (a).

ment of the angular momentum distribution. In particular, many particles acquire sufficient angular momentum to carry them beyond the outer edge of the grid, at which point they are discarded from the calculation. Few particles are lost at first, merely 2.4 per cent by time 50, but 17 per cent have gone by time 103 and many more seem destined to leave soon afterwards. This could be caused by the edge instability.

Because of these uncomfortably large losses, we ran the calculation a second time, but with the initial disc scale halved with respect to the grid dimensions and the outer cut-off now set at $r=6a$.

We also used twice the length of time-step. The behaviour was rather similar. The bar formed at about the same epoch and initially rotated at the same rate, but the more extended active outer disc was able to accept yet more angular momentum from the bar, whose pattern speed at equivalent later times was lower as a result. There was also a suggestion of an $m=1$ instability in the outer parts of this more extensive model, which became noticeably lop-sided by time 100. Despite this, only 0.5 per cent of the particles had left the grid by time 112.

We have chosen to study the bar of the first model, rather than that of the second, for a number of reasons. The strength of the $m=1$ component of the force field was weaker and our knowledge of the bar properties is of higher quality – the bar extends over more grid points and contains more particles.

3 Global properties of the bar

3.1 SURFACE DENSITY DISTRIBUTION

Fig. 4(a) shows contours of the surface density of particles in the model averaged over 13 moments from times 91 to 103 – each was rotated so that the bar major axis was horizontal before averaging. In Fig. 4(b) the projected bulge volume density has been added to the average disc surface density. Fig. 5 gives the density profiles along and perpendicular to the bar major axis, both with and without the bulge.

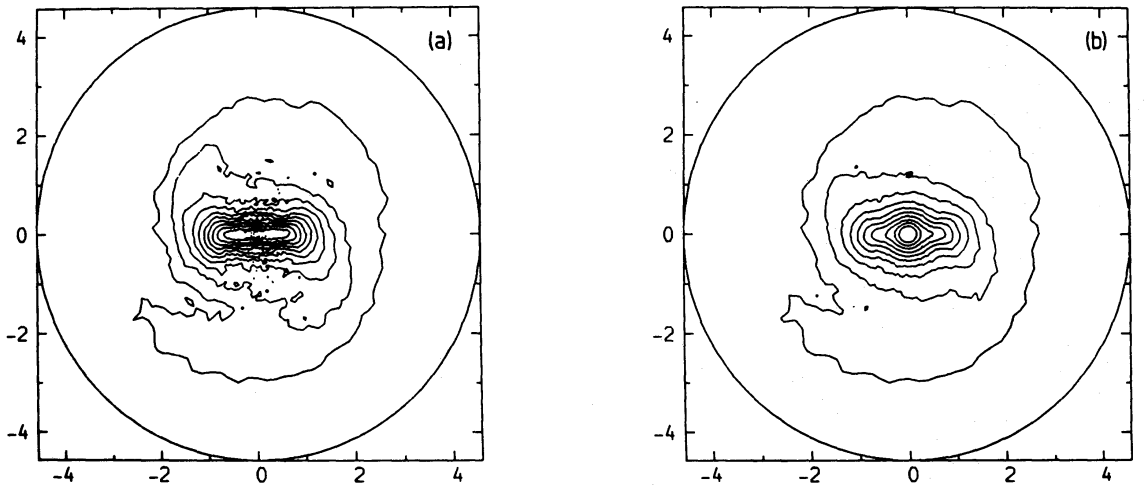

Figure 4. (a) Contours of surface density of disc particles in the model averaged over times 91 to 103. The outer circle marks the edge of the grid and contour values are spaced at equal values in the logarithm, from 0.005 to 0.2. Note that the bar contours are box-shaped rather than elliptical. (b) The same disc mass distribution, but with the projected density of the bulge component added; contour levels run from 0.005 to 1.0 at equal logarithmic intervals.

The most notable feature of the bar is its almost rectangular shape; density contours are far from the ellipses commonly assumed for model bars. In order to demonstrate that this is quite realistic, we compare our model to the SB0 galaxy NGC 936. Fig. 6(a) shows Kormendy's isophote map for this galaxy and Fig. 6(b) the projected surface density of our model, with the bulge included, when 'observed' at the angle we see NGC 936. (Of course, these can be compared only if we assume that the mass-to-light ratios of the bulge and disc are equal and independent of radius, and that there is no internal extinction. These assumptions may not be too implausible for such an early-type galaxy.) The similarity of contour shapes is quite striking.

1987MNRAS.225..653S

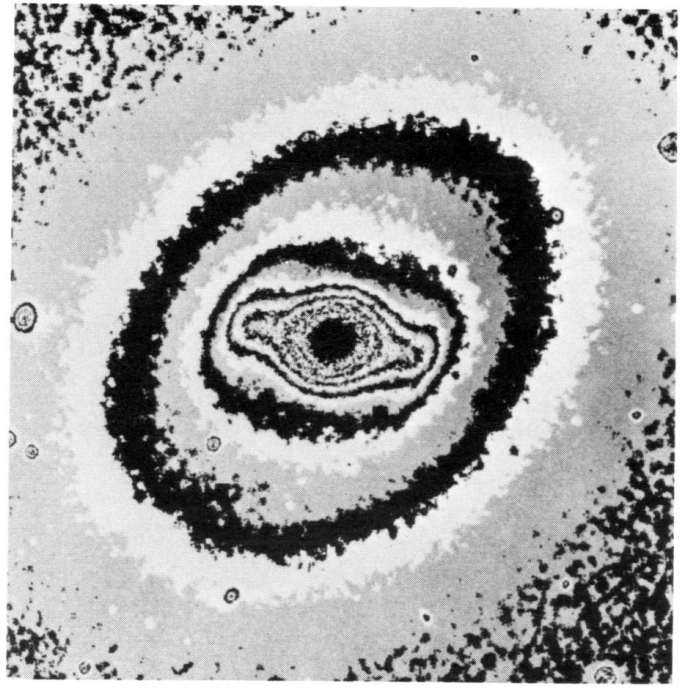

(a)

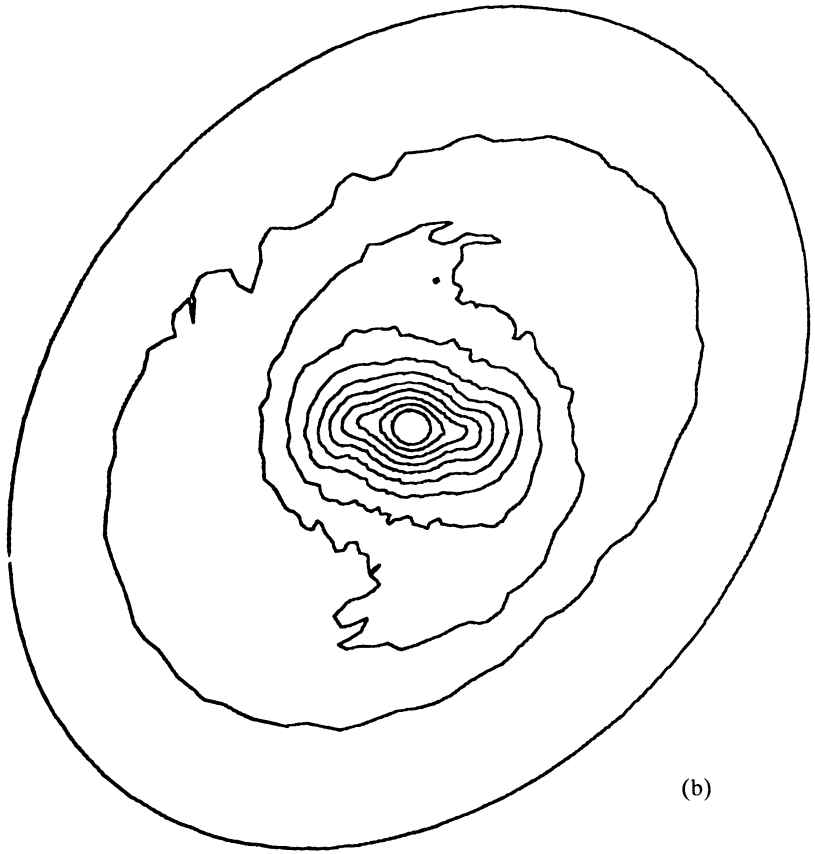

(b)

Figure 6. (a) An isophote map of NGC 936 reproduced from Kormendy (1983). (b) Contours of surface density of the model bulge and barred disc projected to the viewing angles of NGC 936. The bar lies at 65° from the line of nodes, about which the disc is tipped by 41° away from face-on. The contours are spaced logarithmically from 0.005 to 1.0.

[*facing page* 658]

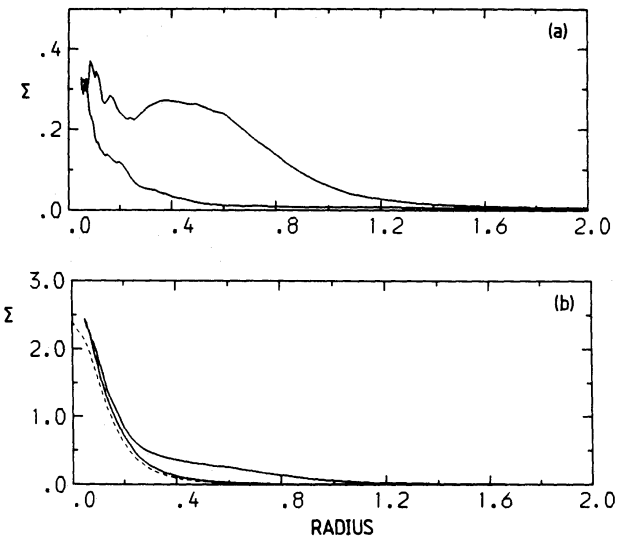

Figure 5. Profiles of surface density along and perpendicular to the bar. In (a) the bulge component is neglected, but it is included in (b) and shown separately by the dashed line.

3.2 VELOCITY FIELD

The magnitude and direction of the streaming motion vector, viewed from a frame corotating with the bar pattern, is shown in Fig. 7. This is determined from the motions of the particles in each of 25 radial and 12 angular bins. The stars within the bar stream faster than the figure, whereas those outside are slower. Moreover, the streamlines within the bar are highly elongated, while those far out are much less so. Similar behaviour has been reported previously for other model bars and Kormendy's (1983) measurements for NGC 936 indicate that the stars in that barred galaxy stream in a similar fashion.

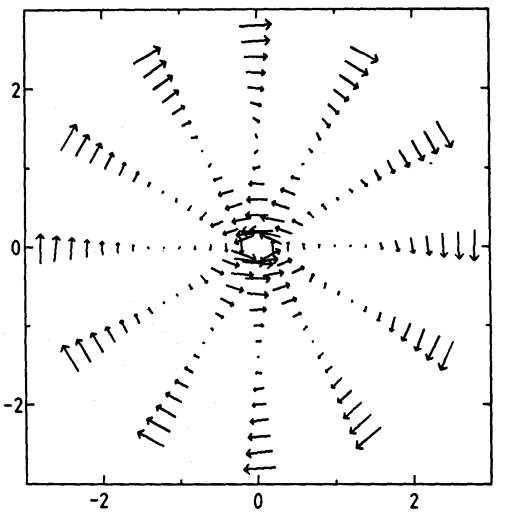

Figure 7. The velocity field of the disc particles in the model at time 90, viewed from a frame corotating with the bar. The arrows indicate the magnitude and direction of the mean streaming speed in each bin. Within the barred region the stars stream faster than the pattern, whereas outside their mean motion is slower.

Fig. 8 shows the stream speed and velocity dispersion in our model as they would be measured by an observer from the angle we view NGC 936. We have simulated three slit positions, along and perpendicular to the bar and along the minor axis of the projected galaxy, using the coordinates of all particles at time 99 lying within a rectangular 'slit' of width of $0.2a$. The

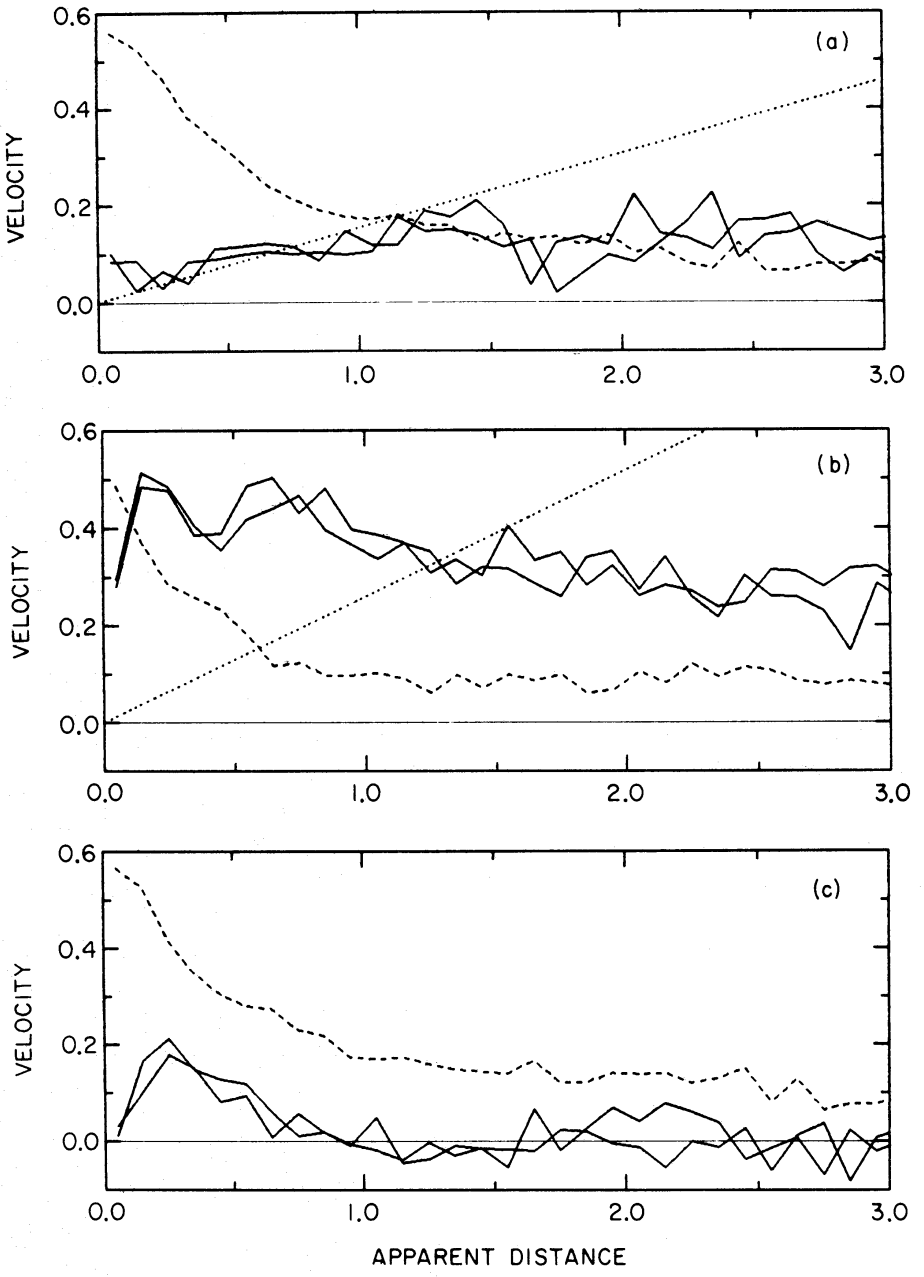

Figure 8. The mean line-of-sight velocity of model disc stars on each side of the centre (solid lines), and the velocity dispersion averaged between the two sides (dashed line), as they would be measured by an observer from the viewing position of Fig. 6(b). The velocities have been added in bins of width 0.1 along a slit of width 0.2 placed (a) along the bar, (b) normal to the bar and (c) along the minor axis of the projected disc. Parts (a) and (c) may be compared with fig. 3 of Kormendy (1983) which shows the corresponding data for NGC 936; one length unit corresponds to approximately 40 arcsec for NGC 936. Note that our model includes no contribution from bulge stars. The light dotted line shows the velocities that would be observed if all stars corotated with the bar.

streaming speeds on the two sides of the galaxy are shown separately, to indicate the degree of symmetry in the model. The velocity dispersion curves show the combined data from both sides, since any asymmetries were too small to be distinguishable. The suggested scale of $a=40$ arcsec gives the model bar the same dimensions as the apparent size of that in NGC 936.

Our measurements differ from Kormendy's (1983) data in two important respects: (i) we find much lower velocity dispersions and higher streaming speeds near the centre, because we neglect

the contribution from bulge stars and, (ii) the streaming speed declines outwards at large radii much more rapidly than is observed in NGC 936. This could indicate that the barred galaxy, unlike our model, is embedded in an extended dark halo.

Other than this, there is a strong similarity between the stellar motions in our model and those for NGC 936. The most striking resemblance is on the minor axis (Fig. 8c) where there is measurable rotation of the same sign within the barred region and changing sign at a projected distance of 1 in our units (=40 arcsec for NGC 936). We would also note that the streaming speed along the bar (Fig. 8a) becomes equal to the dispersion at about the same point (a projected distance of 1.2 *cf.* 40–50 arcsec from Kormendy's data).

4 Structure of particle orbits

4.1 SPLINE FITTING

We wish to study the orbits of particles in a steady, rotating potential well which is as close as possible to that in the simulation. The gravitational potential in the *N*-body model has statistical fluctuations, owing to the finite number of particles, which we have partly removed by averaging the field over a period of time. We have fitted a bi-cubic spline to this time-average to obtain a smooth field in which to integrate orbits. We preferred a spline to an analytic function fit, as it was not clear whether such minor components as the small-amplitude odd harmonics or the weak outer spiral were important features of the potential.

By time 90, the amplitude and pattern speed of the bar had become fairly steady (Section 2). We averaged the grid values of potential, force and density at the 13 moments 91, 92, . . . , 103, the coordinate system being first rotated so that the bar major axis lay along the x-axis as in Fig. 4; i.e. we did not *assume* a uniform figure rotation rate, although this was very nearly so. The average pattern speed of the bar during this period was $\Omega_p=0.436$.

A (2-D) bi-cubic spline approximation was found separately for the mean potential, for the mean forces parallel to the x- and y-axes (along and perpendicular to the bar), and for the mean density of the disc particles; the bulge contribution was added separately. A quasi-Cartesian coordinate system was adopted for the fit:

$$X=s(r)\cos\theta \qquad Y=s(r)\sin\theta$$

where the radial coordinate $s(r)$ is given by

$$s(r)=r \qquad (r<e/c),$$

$$=e\ln(cr)/c \qquad \text{otherwise.}$$

Here, $c=30/a$ and e is the base of natural logarithms. This function has a continuous first derivative at the cross-over radius (here $r=0.09$, at about the 10th radial grid point). It is logarithmic at large radii, so that the radial grid there is evenly spaced in s, but avoids a hole at the centre. The spline was defined by minimizing the weighted sum of squared residuals at each data point, using routine E02DAF from the NAG library. Fitting was performed over a square ($|X|<0.446$, $|Y|<0.446$) in the (X, Y) coordinates, which includes the entire grid region inside $r=4.57a$. There were 26 interior knots (27 panels) in each direction; the knots were spaced so that each panel contained, as nearly as possible, equal numbers of grid points at which values were known. Only the four corner panels were left empty of grid points.

The data at each grid point were given unit weight in the fit. Extra points of low (0.001) weight were placed at the corners of the square, with values there calculated assuming that the force diminished radially as the inverse square; these prevent the spline from oscillating near the edge. The error in the final fitted potential was within 0.001 (0.2 per cent of the maximum value) at all

the grid points; the forces were less well approximated, with errors of up to 2 per cent of the maximum value in the major-axis force, and 1 per cent in the minor-axis force. The forces and potential obtained from the spline have continuous second derivatives.

Since the potential and the forces were separately derived during the N-body run, and spline fits were made independently, conservation laws cannot hold exactly for an orbit integrated according to the smoothed forces. In a potential which rotates steadily at the rate Ω_p, energy is not conserved, but the Jacobi constant $J=E-\Omega_p h$ (where E and h are the specific energy and angular momentum) should be constant along an orbit. Measured changes in J serve as a check on the spline fit. These errors are usually below 1 per cent, and always below 2.5 per cent, for integrations lasting 500–1000 time units; they do not seem to accumulate over time, or to be predominantly of one sign. Thus the spline fit is good enough to follow most regular orbits in the potential without deviations becoming large, though it will not be adequate near regions of stochasticity, where the motion is very sensitive to details of the force.

4.2 FAMILIES OF PERIODIC ORBITS

We have searched for particle orbits which close in a reference frame rotating with the bar. Because we were interested mainly in the structure of the bar, we did not investigate orbits outside corotation.

Fig. 9 shows part of the characteristic diagram; the distance at which each orbit crosses the minor axis of the bar is plotted against the value of the Jacobi constant. Here, we plot the y-coordinate (see Fig. 4) as the particle crosses the y-axis (bar minor axis) with $\dot{x}<0$; thus distances associated with orbits in retrograde motion in the rotating frame are shown as negative.

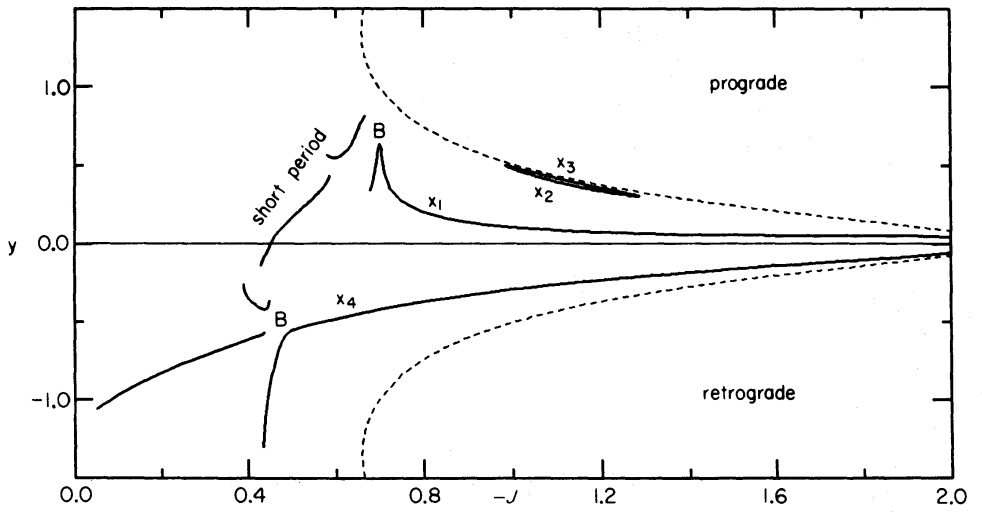

Figure 9. Characteristic diagram for periodic orbits within the bar. The radius at which the orbit crosses the minor (y-) axis with $\dot{x}<0$ is plotted against the value of the Jacobi constant J. The zero-velocity curve, bounding the region accessible to orbits of given J, is shown as a dashed line, and bifurcation points are marked B.

The Jacobi constant (or energy with respect to rotating axes) determines the region accessible to a particle. Particles with small J (to the right in Fig. 9) are confined either deep inside the bar (low angular momentum *and* energy) or far outside the bar (where the angular momentum term dominates J). The dashed curves mark the boundaries of the accessible region where particles would be at rest on the minor axis in the rotating frame. Only those particles having the critical value of J, here $J\simeq-0.7$, may pass through the Lagrange points L_1, L_2 on the major axis (at $x=\pm1.5$); a slightly higher value of J ($=-0.66$) is needed to reach the Lagrange points L_4, L_5 on

the minor axis (at $y=\pm 1.35$). Thus, particles with $J>-0.7$ can cross between the disc and the bar through the saddle points, while only those having $J>-0.66$ are completely unconstrained energetically.

At the lowest energies, there is a family of prograde orbits elongated along the bar (x_1), and a family of roughly circular retrograde orbits (x_4). The shapes of these are shown in Fig. 10(a) and (d). (There are various conventions for labelling the orbit families; ours is that most clearly described by Papayannopoulos & Petrou 1983.)

At higher energies, two more families (x_2 and x_3) of direct orbits appear, both elongated perpendicular to the bar (Fig. 10c). In a weakly barred potential, such orbits arise between the two inner Lindblad resonances as a 2:1 bifurcation of the x_1 family (Contopoulos & Papayannopoulos 1980). The appearance of these two orbit families defines a generalization of the inner Lindblad resonance for a strong bar (van Albada & Sanders 1982). As the bar strengthens, the radial range where these families are found shrinks and they are likely to disappear altogether for rapidly rotating strong bars. It is, therefore, slightly surprising to find them here, even though the bar pattern speed is low enough (see Fig. 3b). However, they are only just present – the loop of the x_2, x_3 orbits in Fig. 9 is squashed up against the zero-velocity curve and encloses a very small area.

At larger values of the Jacobi constant, the x_1 family extends to larger radii, and the orbits develop loops at the ends (Fig. 10a). Eventually this family undergoes a 3:1 bifurcation at the point marked B, and develops the three-cornered shape shown in Fig. 10(b). We could trace only one branch of this family after the bifurcation, though three should be present (Contopoulos 1981). This family does not have a 1:1 bifurcation inside corotation.

At yet higher energies, there are the short-period orbits around the minor axis Lagrange points (Contopoulos 1978). Because the bar is not exactly symmetric, this family is split into two disconnected pieces; the asymmetry is evident in the shapes of the orbits [Fig. 10(e) and (f)]. The banana-shaped long-period orbits, which are frequently unstable (Contopoulos 1983a), could not be found, probably because of limitations in our spline fit. Orbits in the vicinity of the Lagrange points have very long periods, making them extremely sensitive to details in the force field, so it is not surprising that we experienced difficulty in locating periodic orbits for $J\simeq -0.7$. We could not follow the x_1 family beyond its first bifurcation.

The x_4 (retrograde) family undergoes a 1:1 bifurcation at about $J=-0.45$; orbits on the uppermost and lowermost branches have their centres displaced along the major axis, as shown in Fig. 10(d). The gap between the various branches of this family appears to be real although no previous study has noted such a gap. It could be due either to the small asymmetries in our potential or simply that our spline fit prevented us from tracing the family along its entire length.

Again due to the shortcomings of the spline fit, we could not determine the stability of most of these orbits. The x_1 family is stable at energies below that of the 3:1 bifurcation, and the x_4 family is stable below its 1:1 bifurcation. The central portion of the x_2 family is stable and that of the x_3 family is unstable. This is exactly as expected from the previous studies cited above. In other cases, the results of the stability analysis are inconclusive.

In summary, the periodic orbits found here differ very little from those in the bar potentials studied elsewhere. The only difference which might be significant is that in this bar, the long-axis orbits develop only very small loops at their ends, in contrast to the much larger loops usually found in ellipsoidal bar potentials (e.g. Contopoulos 1978; Papayannopoulos & Petrou 1983; Teuben & Sanders 1985 – but see Athanassoula *et al.* 1983).

4.3 ORBITS OF BAR PARTICLES

The set of periodic orbits in the bar is very much smaller than the set of all possible orbits, but we

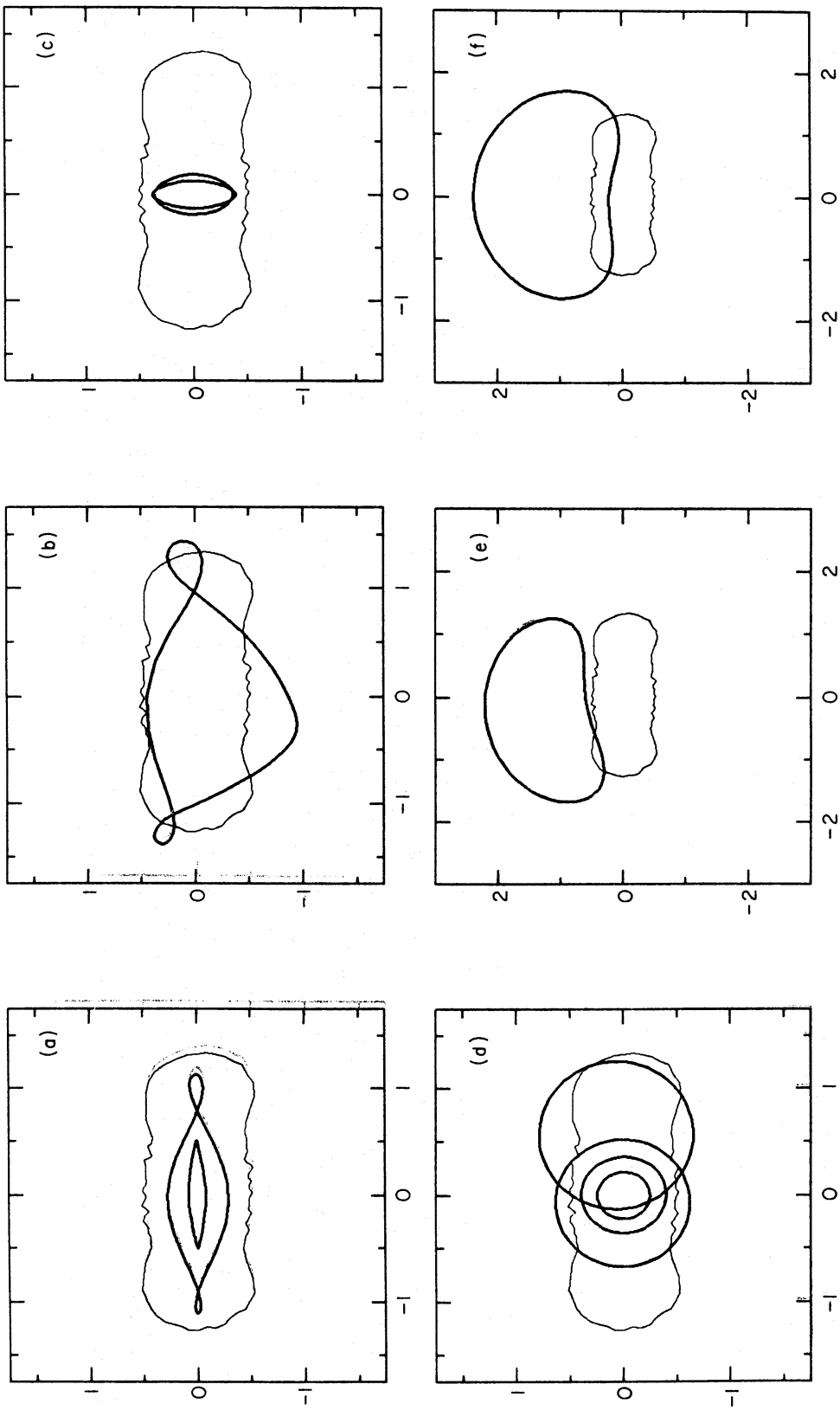

Figure 10. The shapes of some periodic orbits (heavy lines). The light line is a contour of constant surface density in the barred disc (at a value of 0.02) to indicate the size of the bar; note that the scale varies between pictures. (a) x_1 (long-axis) orbits; the smaller has $J=-1.15$, the larger $J=-0.75$. (b) An x_1 orbit for $J=-0.69$, beyond the 3:1 bifurcation. (c) Two orbits from the perpendicular families at $J=-1.15$; the rounder is x_2 and the narrower is x_3. (d) Several retrograde (x_4) orbits. Their Jacobi values are, in order of increasing radius: -1.15, -0.75 and -0.4 (twice). The off-centre orbit lies on the upper branch of the x_4 family after all its 1:1 bifurcation. (e) A short period orbit with $J=-0.6313$ and (f) another with $J=-0.525$.

expect many particles to oscillate about a periodic orbit, following it with limited deviations. This would imply that the general properties of orbits within the bar will be closely related to those of the periodic orbits about which this trapping occurs; for example, orbits trapped near the x_1 (long-axis) family tend to stream round faster than the figure rotation, while those trapped around the x_4 (retrograde) orbits will contribute to counter-streaming motions. Some idea of the character of the orbits of the particles in the simulation may be obtained from the streaming motions illustrated in Fig. 7, but a clearer picture emerges if we construct surfaces of section.

A diagram such as Fig. 11(a) records the values of $(y, \dot{y})$ for each orbit, each time it crosses the minor (y-) axis with $\dot{x}<0$. Particles in prograde motion in the frame of the bar have $y>0$ when $\dot{x}<0$; particles in retrograde motion in the bar frame have $y<0$. In this figure, a simple periodic orbit – which always crosses the minor axis at the same place and with the same velocity – is represented by a single point. A doubly periodic orbit, circling the bar twice before it closes, appears as two points, and so on. A regular orbit, which behaves as if it respects two integrals of motion (i.e. not only the Jacobi constant), generates a closed invariant curve, while an irregular orbit covers a finite area in the surface of section (see e.g. Binney 1982 for a general discussion).

The invariant curves generated by a regular orbit cannot be crossed. Thus if the starting point in the surface of section for an irregular orbit lies between two closed invariant curves, the orbit is trapped there, and behaves essentially as a regular orbit. Alternatively, an untrapped irregular orbit may explore all of phase space, outside any invariant curves, which is accessible for that Jacobi constant. There is an intermediate case, of semi-trapped orbits (see Petrou 1984), which remain close to a periodic orbit over many circuits of the bar, but eventually escape, because the barriers (cantori) which confine them are only partial (Percival 1979; Mackay, Meiss & Percival 1984).

Fig. 11(a) shows a surface of section at Jacobi constant $J=-1.15$. The four periodic orbit families x_1, x_2, x_3, x_4 each generate a single point (large dot). The orbits of six particles actually present in the N-body simulation (larger symbols) are shown, along with two other orbits (small symbols). These were selected to illustrate the types of behaviour. Two of the bar particles are on regular or trapped orbits; one (marked with diamonds) about the x_1 orbit, another (plusses) about x_2. No trapping is possible about the x_3 family since it is unstable. The structure of trapped orbits around the x_4 (retrograde) family is shown by two orbits which do not represent bar particles from the simulation. No bar particles oscillate around the x_4 family itself, though we show a particle (triangles) which is trapped near a more complicated doubly periodic retrograde orbit. Two orbits (squares and crosses) are semi-trapped around the x_1 family; apparent bounding cantori are sketched freehand. Finally, we show a completely untrapped orbit (circles) which visits the remaining phase space not occupied by regular or semi-trapped orbits.

Although numerical difficulties prevent us from tracing periodic orbits near stochastic regions, these areas may still be mapped in the surface of section. This is because the sequence of crossing points in the surface of section represents 'typical' behaviour for that region (Hénon 1983). In the stochastic regions, no numerical scheme, however careful, can follow the orbit accurately (see e.g. Merritt 1980). In regions of regular orbits, errors in calculation do not build up quickly and the spline scheme should preserve this regular character.

To obtain a general idea of the orbits followed by the majority of the simulation particles, the paths of 14 000 of them (about 1/3 of the total, chosen at random) were integrated until they first crossed the minor axis of the bar with $\dot{x}<0$. The pair of numbers $(y, \dot{y})$ then gives the first point on a surface of section for that orbit. Fig. 11(b) shows the results in a range of Jacobi constant $-1.2<J<-1.1$, the dashed curve shows the region accessible to particles with $J=-1.15$. Most of the initial points fall inside the outer cantorus of Fig. 11(a); of these, the orbits outside the regular region are semi-trapped about the x_1 family. Trapping about the x_2 family is negligible and there is none about the retrograde orbit x_4. There are few completely untrapped orbits. This supports

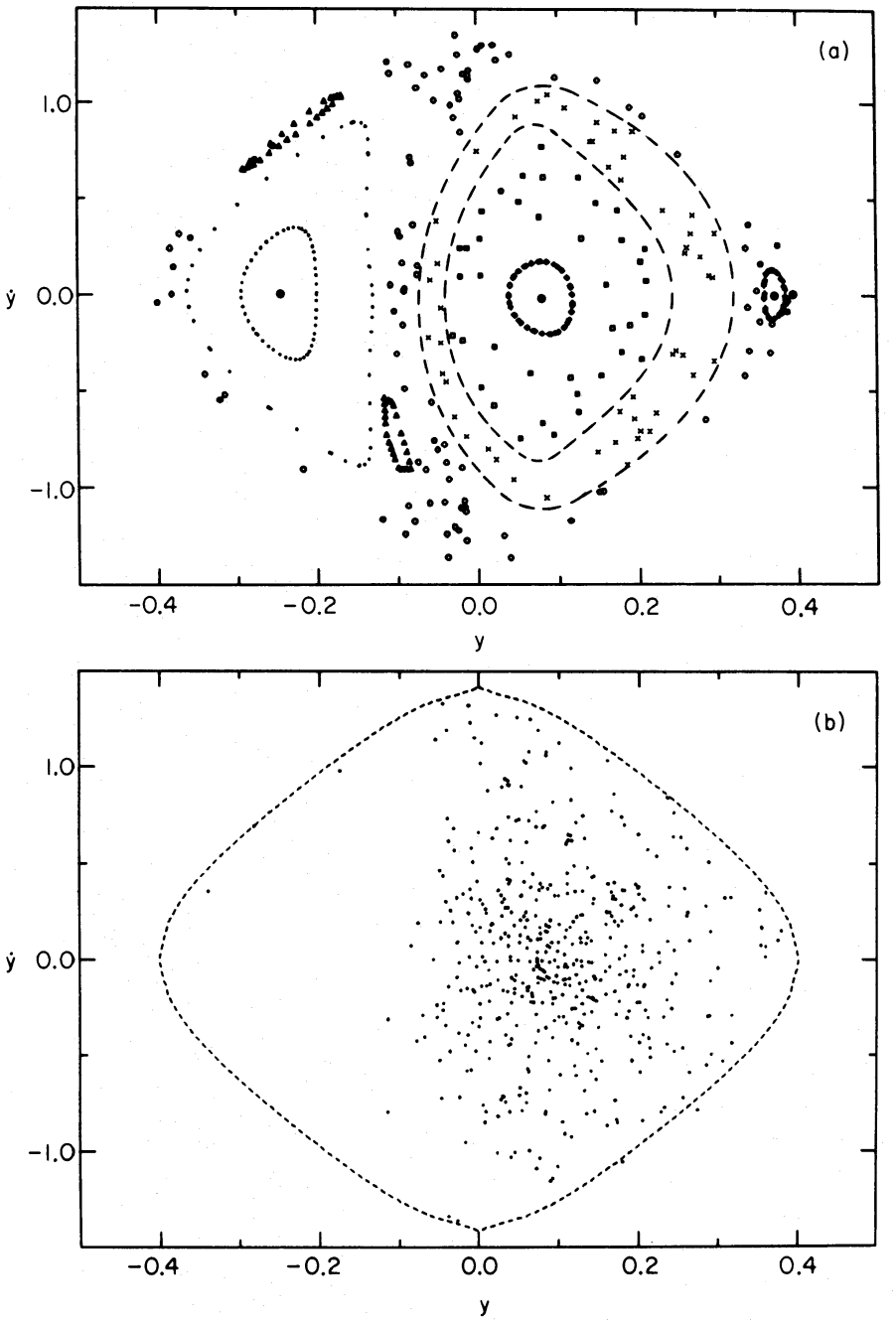

Figure 11. (a) Surface of section for orbits with Jacobi constant $J \simeq -1.15$. As each orbit crosses the minor (y-) axis of the bar with $\dot{x}<0$, the values of $(y, \dot{y})$ are plotted. The four simple periodic orbits are shown as filled circles. The two regular retrograde orbits shown do not correspond to particles in the simulation, but the behaviour of six particles in the simulation is shown by the larger symbols. Two cantori are sketched as dashed lines. (b) Minor axis crossing points for 502 particles having Jacobi constants in the range $-1.2<J<-1.1$ at time 99. The point $(y, \dot{y})$ is plotted for each orbit on the first crossing with $\dot{x}<0$. The dashed curve shows the boundary of the region accessible at $J=-1.15$. Note that very few of the particles are retrograde and the great majority lie inside the outer cantorus shown in (a).

Petrou's (1984) conjecture, that a self-consistent bar may be extensively supported by stars on irregular orbits, provided these are confined for long (though finite) times by partial barriers (cantori).

Fig. 12(a) is similar to Fig. 11(a), but shows orbits at Jacobi constant $J=-0.75$. The only periodic orbits at this energy within the bar are the long-axis x_1 and the retrograde x_4 orbits. A

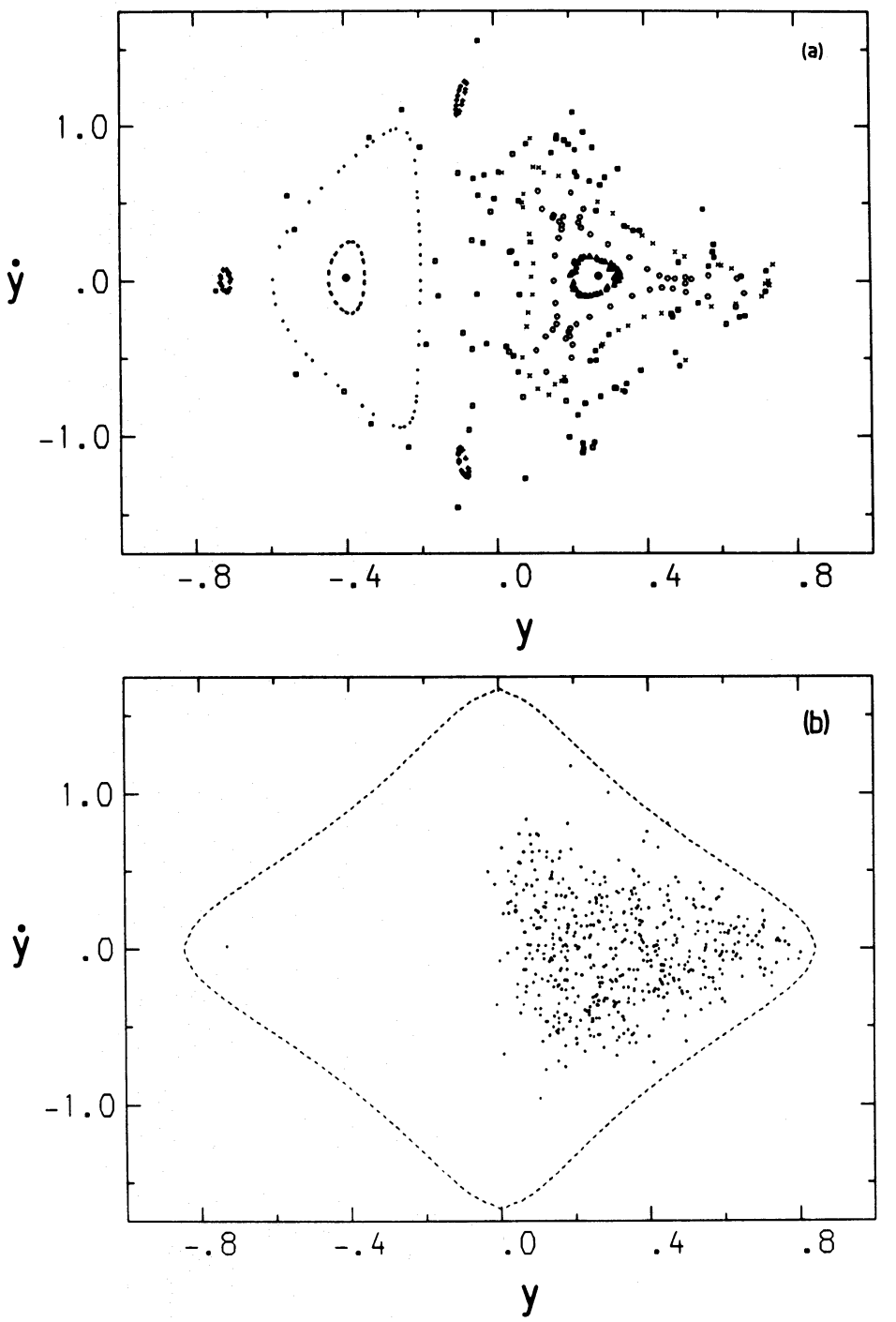

Figure 12. (a) As for Fig. 11(a) but at Jacobi constant $J=-0.75$. The x_1 and x_4 periodic orbits are marked as filled circles. (b) As for Fig. 11(b), for 522 particles in the range $-0.77<J<-0.73$. Only particles within corotation ($|y|<0$) are shown.

complex structure can be seen; one particle (triangles) stays close to the x_1 orbit, but its own orbit is clearly not regular. Another (circles), while trapped near the long-axis family, is strongly influenced by a triply periodic orbit (which could not itself be traced in our spline potential). The orbit marked with crosses at first appears to be trapped about the x_1 family, but later escapes to explore a larger region, perhaps breaking through a cantorus. One orbit (plusses) is trapped about a triply periodic retrograde orbit. Finally, the orbit marked with squares initially stays close

to a regular orbit about x_4, but then escapes to explore a larger region. By contrast, there is a large region of regularity near the retrograde orbit x_4, but no bar particles are trapped there.

Fig. 12(b) shows the initial points on the surface of section for the orbits of 522 particles with Jacobi constants $-0.77<J<-0.73$ which fall within the bar ($|y|<1.5$). There is only one particle (plusses in Fig. 12a) with significant retrograde motion. Most of the bar population at this Jacobi

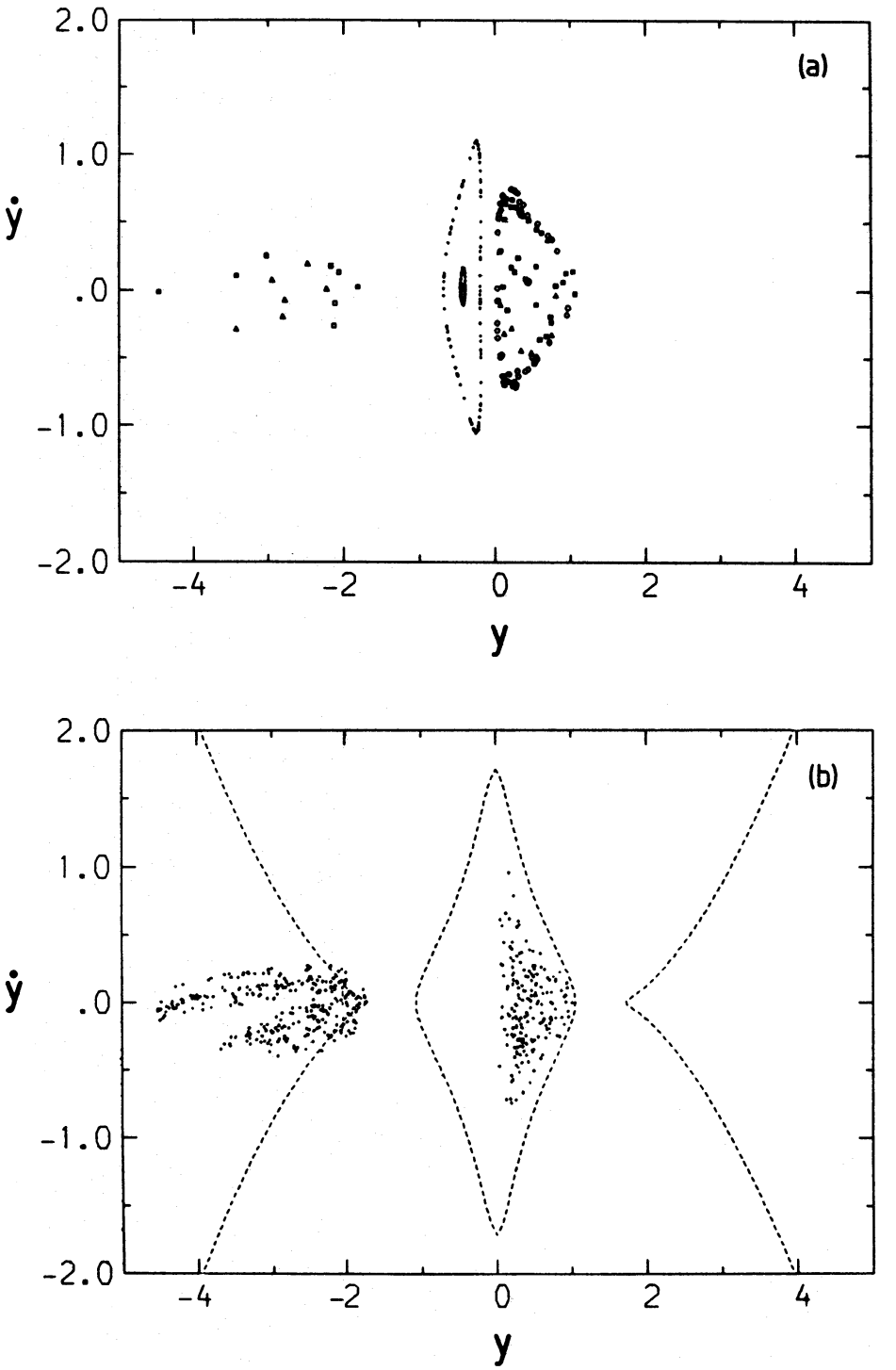

Figure 13. (a) As for Fig. 11(a) but at Jacobi constant $J=-0.69$. The x_1 and x_4 periodic orbits are marked as filled circles. (b) As for Fig. 11(b), for 486 particles in the range $-0.695<J<-0.685$.

value is either trapped or semi-trapped about the x_1 orbit, much as at $J=-1.15$. The points do not fill evenly all the right-hand half of the surface of section permitted at this Jacobi value; the triply periodic direct orbit (near the circles in Fig. 12a) obviously has a strong effect.

When the Jacobi constant rises as high as $J=-0.69$ (Fig. 13), there is a sharp change in behaviour. These particles have enough energy to move between the bar and the disc, though they still cannot reach the Lagrange points L_4, and L_5 on the minor axis. In Fig. 13(a), the orbit marked with circles seems to be regular, forming a one-dimensional closed curve; but this cannot really be a regular orbit, as the other two shown cross it, hopping between the bar ($y>0$) and the disc ($y<0$). (Fig. 15 shows part of the path of the orbit marked with squares.) One of the squares falls nearly on top of that of the x_1 periodic orbit, showing that the x_1 orbit now has at best a very small island of trapped orbits around it, and may actually be unstable.

Fig. 13(b) shows the initial points for the orbits of 486 bar particles with $-0.695<J<-0.685$. None fall in the range $-1.5<y<0$, which corresponds to particles within the bar but rotating more slowly than the figure. Of 38 orbits examined in the range $-0.695<J<-0.685$, 35 showed the 'hopping' behaviour while the other three behaved like the orbit marked with circles in Fig. 13(a). Thus most of the particles in this energy range move between the disc and the bar; some remain within the bar, on orbits streaming faster than the figure rotation, and the rest must stay in the outer disc. There is no population which is confined within the corotation radius, but which reverses its sense of streaming relative to the bar. On the left-hand side of the figure, orbits with large values of $|\dot{y}|$ are absent; these would have large angular momenta and energy, and would not be bound to the model.

The transition between the behaviour seen in Figs 11 and 12 and that displayed here occurs fairly abruptly around $J=-0.7\pm0.005$. This is both the minimum value required to escape along the major axis of the bar [at the L_1 point ($x=1.51, y=0$), the minimum Jacobi constant is -0.705], and the energy at which the x_1 orbit family undergoes its 3:1 bifurcation. Contopoulos (1983b) suggests that in a strong bar, stochasticity may become important at the 3:1 bifurcation, so that the bar must end inside corotation, at about the maximum radius reached by orbits of the x_1 family before the bifurcation. We cannot distinguish here between this possibility and the hypothesis that bars extend to corotation.

A number of authors (Petrou 1984; Teuben & Sanders 1985; Pfenniger 1985) have found that strong stochasticity appears in various barred potentials at a Jacobi value significantly below that required to reach corotation. Particles on these stochastic orbits intermittently reverse their sense of streaming relative to the bar pattern, and the average density associated with them is much nearer to axisymmetric than is the bar density. Thus a lens structure, ending at corotation, may be built up. There is no such population in this model; all particles which are confined within the bar are semi-trapped and must stream faster than the pattern, and there is no sign of a lens in Fig. 1.

The particles can be split into three populations having the spatial distributions shown in Fig. 14. A typical orbit from each of these is shown in Fig. 15.

(i) Bar particles have low Jacobi constants and are confined to the bar. Almost without exception, they orbit faster than the pattern rotation rate and are trapped or semi-trapped about the long-axis x_1 family of periodic orbits. The orbit of the bar particle with $J=-0.71$ is one of many that fill out the square ends of the overall bar shape.

(ii) Disc particles also have low J but are excluded from the bar. They are on near-circular orbits outside the bar. The orbit shown has the same J as the bar particle in (i).

(iii) A 'hot' population of particles (with $J>-0.7$) can wander throughout the system. These particles are on eccentric orbits which can carry them both into the bar and far out into the disc. The particle with $J=-0.69$ (squares in Fig. 13) moves in and out of the bar through the major axis Lagrange points (L_1 and L_2) even though it has insufficient energy to reach L_4 or L_5.

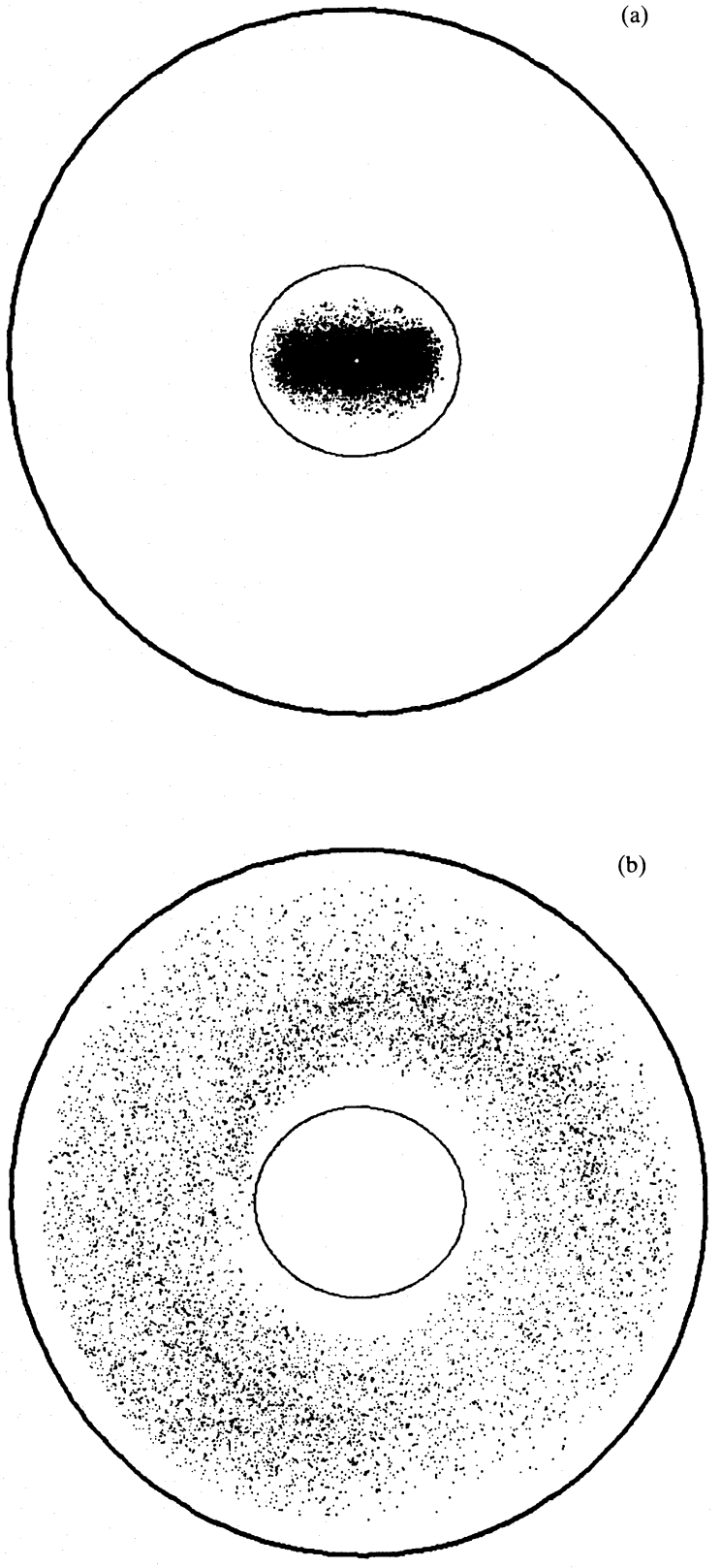

Figure 14. The positions of all particles of each of (a) the bar, (b) the disc and (c) the 'hot' populations at time 99. The ellipse is drawn through all four Lagrange points.

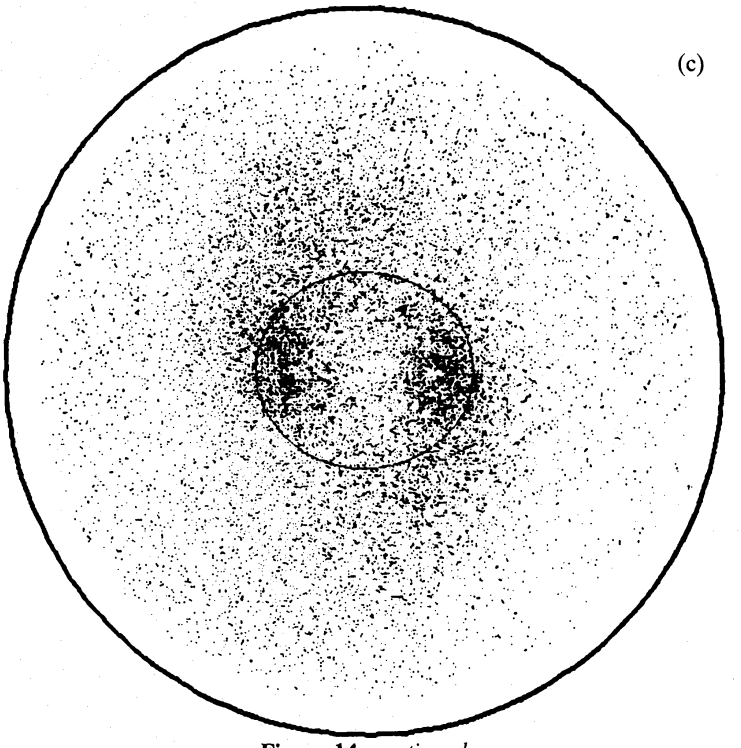

Figure 14–*continued*

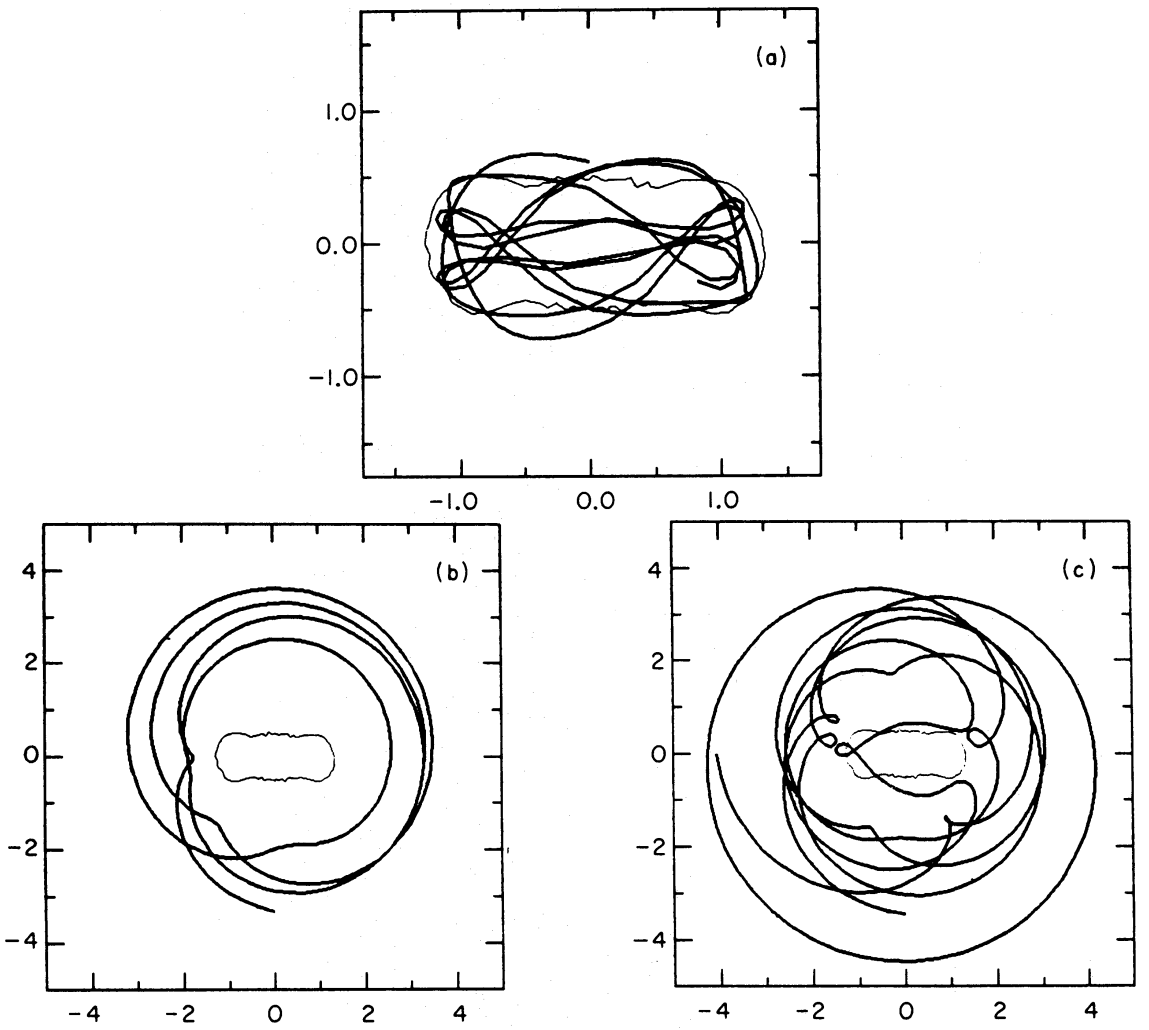

Figure 15. The three types of orbit in the model: (a) an orbit trapped within the bar, (b) an orbit of the same Jacobi constant ($J=-0.71$) confined to the disc, and (c) an orbit with sufficient energy ($J=-0.69$) to cross the Lagrange points (shown by the squares in Fig. 13a). The light line in each shows a disc surface density contour (at 0.02) to indicate the approximate size of the bar.

5 The stability of the bar

We have so far demonstrated that our N-body bar was supported, as expected, by the main long-axis family of orbits. In this section we show that it is remarkably robust and appears to be in equilibrium.

5.1 SEPARATING THE BAR FROM THE DISC

The disc instability guaranteed a self-consistent rapidly tumbling bar, surrounded by an outer disc of stars such as might be present in barred galaxies. The spiral arms, which persist in this realistic situation, remove angular momentum from the bar particles, causing the properties of the bar to change. Any secular evolution the bar itself may wish to undergo would be masked by these forced changes. To prevent this, we froze the disc and 'hot' populations of particles (Fig. 14b and c). The axially symmetrized gravitational field of these frozen particles, together with that of the bulge, supplemented the radial component of force felt by each remaining particle.

A particle remained mobile only if its Jacobi constant was less than a certain value, J_c, and it lay within an ellipse passing through the Lagrange points L_1 and L_2 (at $y=\pm 1.3$ on the minor axis) and L_4 and L_5 (at $x=\pm 1.5$ on the major axis). We experimented with three values of J_c in the range -0.695 to -0.75. The highest value was chosen to select the entire population of 17 068 bar particles (Fig. 14a). The lower values discard some of these also: only 14 565 particles remain after the deepest cut.

Since few particles reach radii beyond $r=2$, it seemed wasteful to use the original linear scaling to the grid dimensions. We therefore doubled the dimensions of the bar with respect to the grid for most of these calculations, although we checked that when the original numerical parameters were retained, we obtained very similar results.

5.2 ROBUSTNESS

We ran eight further simulations in which the bar was isolated in this way, which demonstrate that it is remarkably robust. The differences between these models are summarized in Table 1. In every case, except that in which all tangential forces were suppressed, the bar showed almost no tendency to dissolve.

This is quite remarkable. Our prescription for selecting the bar particles suddenly removes the contribution to the non-axisymmetric gravitational field from the disc and 'hot' populations (Fig. 14b and c). The models with cuts at lower values of J_c were changed even more drastically, yet

Table 1. Models of the isolated bar. The columns give: the maximum value of the Jacobi constant of the particles used in each simulation, the number of particles selected, the time-step and grid scaling used, the Fourier harmonics contributing to the force determination, the duration of each run and the initial pattern speed.

J_{max}	N	Time-step	Grid scaling	Fourier components	Duration	Ω_p
−0.695	17 068	0.01	Double	0–9 inc	50	0.412
−0.705	16 533	0.02	Old	0–9 inc	40	0.407
−0.75	14 565	0.01	Double	0–9 inc	50	0.411
−0.695	17 068	0.01	Double	0+2+4+6+8	25	0.412
−0.695	17 068	0.01	Double	0+2 only	50	0.401
−0.695	17 068	0.01	Double	0 only	60	(No pattern)
−0.695	17 068	0.02	Old	0–9 inc	50	0.408
−0.695	17 068	0.004	Double	0–9 inc	50	0.421

each time the bar survives the operation with scarcely a quiver! Apparently, discarding the most energetic 15 per cent of the particles from a bar gives another equally stable one.

These experiments also demonstrate that the odd Fourier components are totally unimportant. The bar was unaffected when the odd harmonics of the force field were suppressed and survived when only $m=2$ remained active, although its pattern speed was a little different. Note that in this case the bar is not at all self-consistent, since the density distribution retained strong higher Fourier harmonics, even though the non-axisymmetric part of the forces were strictly $m=2$.

5.3 PATTERN SPEEDS

The pattern speed of the bar in each case (given in Table 1) is substantially (between 5 and 7 per cent) lower than the final value (0.436) in the original model with the outer disc active. There are at least two reasons for this discontinuity: first, some particles contributing to the bar are removed, and secondly, the orbits of the remaining particles must be somewhat different in the new gravitational potential.

The bar is a non-linear density wave in which the lines of apsides of all the orbits are constrained, by the non-axisymmetric forces, to turn at the same rate (on average) – the pattern speed. The figure rotation rate adopted must be a democratic compromise between those particles whose unforced rate of precession is higher than average and those which would prefer to turn more slowly. The stars of the hot population, which contributed to the bar for part of their orbits, were removed suddenly and it seems likely that they were a group urging the bar to rotate faster.

The unforced rate of turning of the line of apsides of an orbit is a function of both its mean radius and eccentricity (or energy and angular momentum) (e.g. Lynden-Bell 1979). In order to ascertain this quantity for any orbit in the bar, we would have to remove the non-axisymmetric part of the field adiabatically. This experiment, though interesting, would take us well away from the present study.

5.4 STABILITY

There was a small, but easily measurable change in the pattern speed as all these models evolved; the mean pattern speed was typically 1–2 per cent lower in the second half of a run than in the first. The amplitude also declined very slightly, which may be due to loss of particles from the bar – a few (about 1 per cent) get out of the bar during the usual duration of these runs – 50 time units, or about 3.5 bar periods.

However, most of these slow changes can probably be attributed to numerical effects, since the rate of change is reduced as the quality of the calculation is improved. (The most important parameter appeared to be the time-step.) The trend is clearly towards the bar properties remaining constant in a perfect calculation. We ran the model without tangential forces largely to determine the time it would take for the orbits of the particles to phase mix back to a nearly axisymmetric configuration. This was virtually complete within 15 time units, or one bar period, showing that the changes detected in the other models were very slow.

Proving that the bar is totally stationary is difficult for numerical reasons, but it seems unlikely that it can be exactly so. This is because the occupied regions of phase space are not totally regular. As many particles are confined only by cantori, they will gradually leak on to completely stochastic orbits, although this is a very slow process with a time-scale of many hundreds of bar periods. At some epoch, if the bar were to survive long enough, the rate of loss of particles to the stochastic regions might be balanced by the rate at which stochastic particles pass back through the cantori to become trapped for long periods. If this were to happen the bar could then be

regarded as truly stationary. It would be impossible to demonstrate the slow changes associated with these processes in any conceivable *N*-body code, but they would be of academic interest only: most galactic bars will have tumbled a few tens of times only since their formation.

6 Conclusions

The principal conclusions of this work are:

(i) The rapidly tumbling *N*-body bar, formed in an unstable disc, has many of the properties of bars observed in real galaxies.

(ii) The barred potential supports many of the well-known families of periodic orbits found previously in rotating bar-like potentials.

(iii) The bar is composed principally of particles trapped or semi-trapped about the basic long axis (x_1) family of orbits. This is hardly surprising, but the number of particles trapped around the other families is impressively small.

(iv) The bar appears to be quite stable and suffers no detectable secular changes for many tumbling periods, when isolated from the disc, although we cannot rule out the possibility of evolution on a time-scale of hundreds of bar periods.

(v) The bar is also very robust – it was able to withstand substantial surgery, merely adjusting to a slightly different, but also stable equilibrium, after every imposed change.

Our conclusions contrast sharply with Schwarzschild's failure to find a self-consistent rapidly tumbling bar solution using a linear programming technique. We can identify at least two reasons for this: first, the almost total dominance of one orbit family in our bar suggests that the set of self-consistent solutions for any bar model may be small. This would make it unlikely that an arbitrary density distribution and a guessed figure rotation speed could correspond to a self-consistent solution.

Secondly, the density distribution of our bar model was quite decidedly rectangular, not at all like the elliptical figure shapes commonly assumed as bar models. One of the principal difficulties encountered by Schwarzschild was that the orbits in his potential, especially those reaching close to the ends of the bar, had broad loops (private communication). Thus, a self-consistent, rapidly tumbling bar with elliptical density contours may be hard to create. It is quite natural to assume elliptical density contours for models of elliptical galaxies, but it appears to be unwise for rapidly tumbling bars such as are believed to be present in barred disc galaxies. Here the squarer shape of our bar may be required for dynamical reasons, and also apparently corresponds well to the observed isophotal shapes.

The principal limitation of our study is that it was strictly 2-D, the particles were confined to move in one plane as a necessary simplifying approximation for the *N*-body simulation. Pfenniger (1984a) finds complex orbital instabilities in an assumed rapidly tumbling tri-axial bar potential, arising from the coupling of resonances in the principal plane to those normal to it. If a large fraction of phase space were ergodic due to these 3-D unstable orbits, our 2-D model would be seriously inadequate, since the mass distribution could not remain highly flattened. However, the existence of these 3-D instability 'strips' will depend on the degree of flattening and the figure rotation rate, and may be avoidable altogether. Indeed we believe that this is likely to be the case for barred galaxies, since they appear to be very flattened and therefore highly tri-axial. No photometric evidence exists to support this statement, because galaxies are always seen in projection. (A rather doubtful case was argued by Wakamatsu & Hamabe 1984). However, some 30 per cent of edge-on disc galaxies is likely to be strongly barred, yet very few are thick. Thus it seems likely that real bars are at least as thin as the discs in which they formed.

We have not demonstrated that rapidly tumbling bars can exist in isolation. Our bar has a dense bulge at its centre and is surrounded by an extensive disc. It may be more difficult, or even

impossible, for a truly isolated bar to survive indefinitely. Our experiments with the disc particles frozen demonstrated that a bar can survive with no particles energetic enough to cross even the major axis Lagrange points. It seems to us unlikely that the disc potential is really essential for the bar's survival, but we have no proof. This belief would be confirmed once a fully self-consistent bar is constructed by a theorist, but we doubt that it would have any counterpart in nature; it is inconceivable that such a stellar system could form in isolation with nothing 'left over'.

Acknowledgments

We thank M. Schwarzschild and R. H. Sanders for very helpful discussions and G. Contopolous and R. G. Carlberg for comments on the manuscript. LSS acknowledges support from New Hall, Cambridge and the Royal Society; both authors were also supported for part of the time by the SERC. The computations were performed on the STARLINK VAX on Cambridge, and the CYBER 176 in Groningen.

References

Athanassoula, E. & Sellwood, J. A., 1986. *Mon. Not. R. astr. Soc.*, **221,** 213.
Athanassoula, E., Bienayme, O., Martinet, L. & Pfenniger, D., 1983. *Astr. Astrophys.*, **127,** 349.
Binney, J. J., 1982. Saas-Fee lectures 1981. In: *Morphology and Dynamics of Galaxies,* eds Martinet, L. & Mayor, M., Geneva Observatory.
Carnevali, P., 1983. *Astrophys. J.*, **265,** 701.
Combes, F. & Sanders, R. H., 1981. *Astr. Astrophys.*, **96,** 164.
Contopoulos, G., 1978. *Astr. Astrophys.*, **64,** 323.
Contopoulos, G., 1980. *Astr. Astrophys.*, **81,** 198.
Contopoulos, G., 1981. *Astr. Astrophys.*, **102,** 265.
Contopoulos, G., 1983a. *Celes. Mech.*, **31,** 193.
Contopoulos, G., 1983b. *Astr. Astrophys.*, **117,** 89.
Contopoulos, G. & Papayannopoulos, Th., 1980. *Astr. Astrophys.*, **92,** 33.
Hénon, M., 1983. In: *Chaotic Behaviour of Deterministic Systems, Les Houches Session XXXVI,* p. 53, eds Iooss, G., Helleman, R. H. G. & Stora, R., North Holland, Amsterdam.
Hohl, F., 1971. *Astrophys. J.*, **168,** 343.
Hohl, F. & Zang, T. A., 1979. *Astr. J.*, **84,** 585.
Inagaki, S., Nishida, M. & Sellwood, J. A., 1984. *Mon. Not. R. astr. Soc.*, **210,** 589.
Kormendy, J., 1983. *Astrophys. J.*, **275,** 529.
Lynden-Bell, D., 1979. *Mon. Not. R. astr. Soc.*, **187,** 101.
Mackay, R. S., Meiss, J. D. & Percival, I. C., 1984. *Phys. D.*, **13,** 55.
Merritt, D., 1980. *Astrophys. J. Suppl.*, **43,** 435.
Miller, R. H. & Prendergast, K. H., 1968. *Astrophys. J.*, **151,** 699.
Miller, R. H. & Smith. B. F., 1979. *Astrophys. J.*, **227,** 785.
Papayannopoulos, Th. & Petrou, M., 1983. *Astr. Astrophys.*, **119,** 21.
Percival, I. C., 1979. *Non-linear Dynamics and the Beam-Beam Interaction, Conf. Proc. No. 57,* p. 302, eds Month, M. & Herrera, J. C., American Institute of Physics.
Petrou, M., 1984. *Mon. Not. R. astr. Soc.*, **211,** 283.
Pfenniger, D., 1984a. *Astr. Astrophys.*, **134,** 373.
Pfenniger, D., 1984b. *Astr. Astrophys.*, **141,** 171.
Pfenniger, D., 1985. *Astr. Astrophys.*, **150,** 112.
Schwarzschild, M., 1979. *Astrophys. J.*, **232,** 236.
Sellwood, J. A., 1981. *Astr. Astrophys.*, **99,** 362 (Paper I).
Sellwood, J. A., 1985. *Mon. Not. R. astr. Soc.*, **217,** 127.
Teuben, P. J. & Sanders, R. H., 1985. *Mon. Not. R. astr. Soc.*, **212,** 257.
Toomre, A., 1981. In: *The Structure and Evolution of Normal Galaxies,* eds Fall, S. M. & Lynden-Bell, D., Cambridge University Press.
van Albada, T. S. & Sanders, R. H., 1982. *Mon. Not. R. astr. Soc.*, **201,** 303.
Wakamatsu, K. & Hamabe, M., 1984. *Astrophys. J. Suppl.*, **56,** 283.
Zang, T. A. & Hohl, F., 1978. *Astrophys. J.*, **226,** 521.